Fracture clustering effect on AVOAZ analysis

Xinding Fang, Massachusetts Institute of Technology, currently Chevron Energy Technology Company; Yingcai Zheng, University of Houston; Michael C. Fehler, Massachusetts Institute of Technology.*

Summary

Traditional amplitude variation with offset and azimuth (AVOAZ) analysis for fracture characterization extracts fracture properties through analyzing the characteristics of the reflection amplitude variation with offset and azimuth. Validity of the method relies on its basic assumption that a fractured unit can be viewed as an equivalent anisotropic medium in the vicinity where reflection occurs when the spacing between adjoining fractures is sufficiently small compared to seismic wavelength λ. As a rule of thumb, this assumption is taken to be valid when the fracture spacing is less than λ/10. In fracture characterization using AVOAZ, spatial variation of the fracture properties, such as fracture orientation and spacing, are estimated from the anisotropic parameters (e.g. Thomsen's parameters) that are inverted from amplitude variation with offset (AVO) or amplitude variation with azimuth (AVAZ) analysis. Under the effective medium assumption, diffractions from individual fractures are destructively cancelled and only specular reflections from boundaries of a fractured layer can be observed in seismic data. The effective medium theory has been widely used in fracture characterization and its applicability has been validated through many field applications. However, through 3D numerical simulations, we find that diffractions from fracture clusters can significantly distort the AVOAZ signatures when a fracture system has irregular fracture spacing even though the average fracture spacing is much smaller than a wavelength (e.g., <λ/10). Contamination of diffractions from irregularly spaced fractures on reflection can substantially bias the fracture properties estimated from AVOAZ analysis and may possibly lead to incorrect estimations of fracture properties.

Introduction

The linear slip model of Schoenberg (1980) can be used to represent individual fractures, whose elastic property is determined by the fracture compliance matrix that is a function of fracture surface geometry and infill material properties (Schoenberg and Sayers 1995; Brown and Fang 2012). We simulate the influence of fractures on seismic wave propagation using the effective medium model (EMM) and the discrete fracture model (DFM) separately (Yang et al., 2005). In EMM, a fractured layer is treated as a homogeneous anisotropic layer whose elastic properties are calculated from the given background rock properties, fracture density and fracture compliance (Schoenberg and Sayers 1995). In DFM, individual fractures are modeled as imperfect slip interfaces embedded in the background formation using a finite-difference approach (Coates and Schoenberg, 1995). We investigate the limitation of EMM in AVOAZ analysis through comparing the results obtained from the two different models.

Irregularly spaced fracture model

We assume that fracture spatial distribution follows a power law function and the fracture spacing distribution has the following relationship:

$$D(a) = C \cdot a^n \quad (n \neq 0, C > 0) \tag{1}$$

where C is a constant, a is fracture spacing and n is the power governing the distribution.

To generate a random fracture model with fracture spacing distribution following the power law (1), we set

$$\frac{a^n - a_{\min}^n}{a_{\max}^n - a_{\min}^n} = m \tag{2}$$

where m is a random number within the range of [0, 1], a_{min} and a_{max} are respectively the minimum and maximum values of fracture spacing.

From equation (2), we have

$$a = \left[a_{\min}^n + m \cdot (a_{\max}^n - a_{\min}^n)\right]^{1/n} \tag{3}$$

When n=1, equation (3) represents uniformly random distribution; when n<0, equation (3) gives a power law random distribution.

Numerical modeling

We use equation (3) with n=-1 and a_{min}=5 m and a_{max}=30 m to generate a random fracture model whose fracture spacing follows a power law distribution. Figure 1 shows the distribution of 165 fractures in the model. Squares give the spacing between every two adjoining fractures. The dashed line gives the mean fracture spacing, which is 12 m, and the solid curve is the spacing averaged over a 150 m window. The fracture spacing in the model varies from 5 to 30 m in steps of 2.5 m, which is the grid size in the following simulations. The histogram on the right shows the cumulative distribution of fractures with spacing from 5 to 30 m for bin size 2.5 m. The power law function generates a system of fractures having clustering characteristic. We assume that all fractures are vertical and parallel to the y direction and they have the same normal (Z_N) and tangential (Z_T) fracture compliances, which are set to be 10^{-10} m/Pa. This may represent stiff gas-filled fractures (Daley et al., 2002). P and S-wave velocities of the background matrix are respectively 3 and 1.7 km/s. Density is 2.2 g/cm^3. Figure 2 shows the spatial variations of the Thomsen anisotropic parameters (Thomsen, 1986) $\varepsilon^{(V)}$, $\gamma^{(V)}$ and $\delta^{(V)}$

computed from the local average fracture spacing (black curve in Figure 1). The model exhibits weak anisotropy, as fractures are relatively stiff. The assumption of Z_N=Z_T results in $\varepsilon^{(V)}$=$\delta^{(V)}$, which represents elliptical anisotropy.

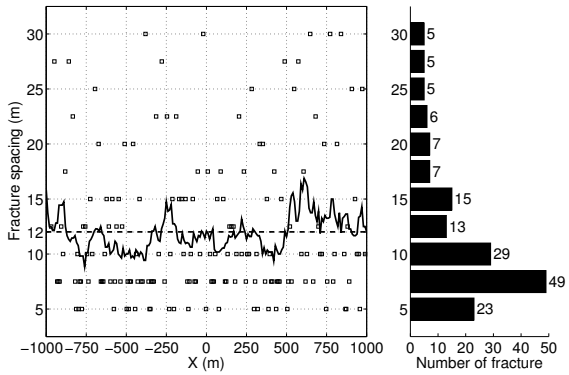

Figure 1: Fracture spacing variation (left) and distribution (right). Squares represent the fracture spacing measured at the mid-point between every two adjoining fractures. Dashed line represents the average fracture spacing (12 m). Solid curve gives the local mean fracture spacing averaged over a 150 m wide window.

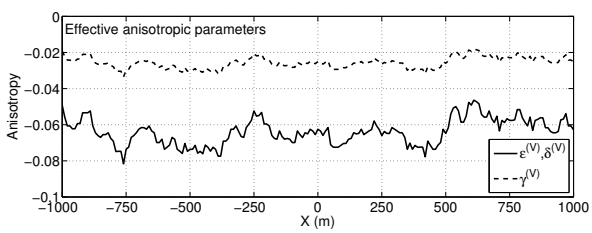

Figure 2. Effective Thomsen anisotropic parameters $\varepsilon^{(V)}$, $\gamma^{(V)}$ and $\delta^{(V)}$ defined with respect to the vertical axis (Rüger, 1997) calculated from the local average fracture spacing.

Figure 3 shows the acquisition geometry. The model dimensions in the x and y directions are respectively 2000 m and 1500 m. A 150 m thick fractured layer extends from 500 to 650 m in depth. Perfectly match layers (PML) are added to all model boundaries. The gray stripes in the fractured layer represent the positions of the vertical fractures that are parallel to the y direction. Common-mid-point (CMP) gathers are collected at 21 positions (red stars) that are located at the center of model y dimension and spread along the x direction from -500 to 500 m in steps of 50 m. In each CMP gather, data are collected at 18 azimuths from 0^0 to 170^0 in steps of 10^0 and at offsets from 300 to 600 m with 100 m interval. Red and blue circles are respectively represent sources and receivers for one CMP. Azimuthal angle is measured from the positive x direction. The strike of fractures is along 90^0. Figure 4 shows comparisons of EMM and DFM for two models with uniform fracture spacing. The fractured layer is modeled as a homogeneously anisotropic layer in EMM when fractures have uniform spacing (Schoenberg and Sayers, 1995). EMM and DFM give identical results when fractures are uniformly spaced and the wavelength is much larger than the fracture spacing. This validates the accuracy of our modeling approaches and the applicability of EMM for equally spaced dense fracture systems.

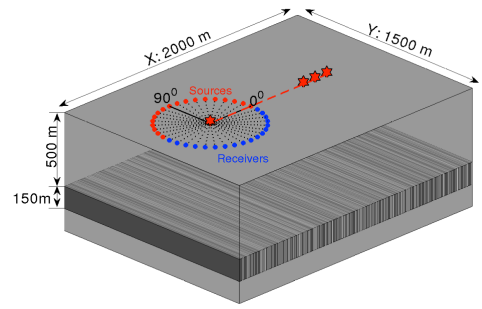

Figure 3: Acquisition geometry.

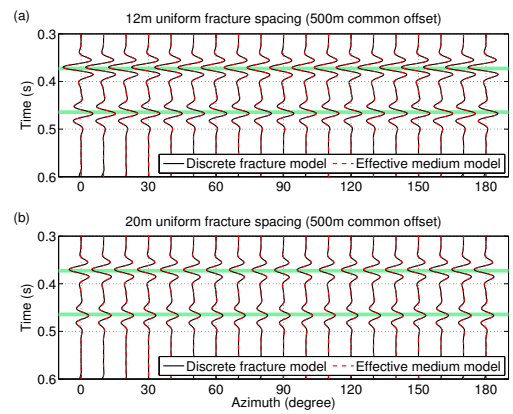

Figure 4: Comparison of the synthetic CMP gathers (pressure) obtained from DFM (black traces) and EMM (red traces) for two scenarios of uniform fracture spacing. The two green stripes in each panel indicate the reflections from the top and bottom of the fractured layer. Source center frequency is 20 Hz.

Figures 5a1-a3 show the shot gathers of the irregular fracture model for sources of different center frequencies. We can see that fracture scattering is prominent even when the source frequency goes down to 10 Hz (λ_P=300m >> fracture spacing). However, fracture scattering becomes very weak when the fracture system has uniform spacing, as shown in Figures 5b1-b3, even for a 40 Hz source. When fractures are irregularly spaced, fracture clusters are sensed by seismic waves as more compliant larger fractures whose effective spacing is much larger than the true fracture spacing. Thus fracture clusters can become strong scatterers even though individual fractures are stiff. This comparison implies that fracture clustering resulting from the irregularly spatial distribution of fractures can generate strong fracture scattering despite the average fracture

spacing being much smaller than the seismic wave length. This provides strong foundation for fracture scattering (Willis et al., 2006; Zheng et al., 2013; Fang et al., 2014) to be an effective method to characterize fractured reservoirs. Figure 6 shows the common offset (at 500m) CMP gathers at three different positions in the model shown in Figure 3 together with the results obtained from EMM. A 20 Hz source was used. The corresponding λ_P is 150 m. The EMM results at each CMP position are calculated based on the effective anisotropy parameters shown in Figure 2. For the top reflections, DFM and EMM results have similar phase and amplitude. However, both phase and amplitude of the results obtained from DFM and EMM are significantly different for the bottom reflections. Figure 7 shows the AVAZ responses extracted from the 500 m common offset CMP gathers at 10 different positions. The AVAZ amplitude is taken as the P-wave (pressure) reflection maximum absolute amplitude. AVAZ of the top reflections obtained from DFM (solid black) follow the expected 'cosine' behavior that is predicted by EMM, although the values of DFM (solid black) differ from those of EMM (dashed black) at most CMP positions. However, AVAZ of the bottom reflections obtained from DFM (solid red) are strongly distorted.

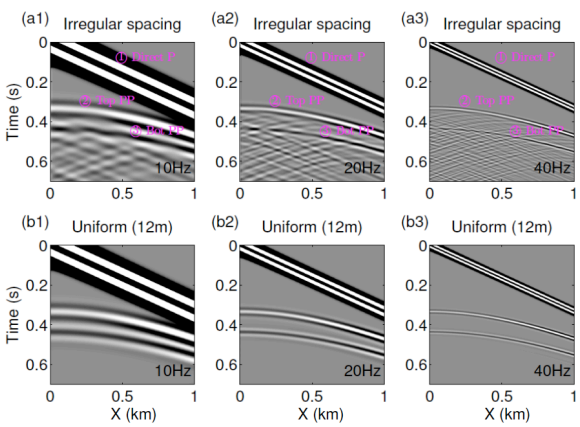

Figure 5: a1-a3 Synthetic shot profiles (pressure) for the irregular fracture model with sources of 10, 20 and 40 Hz frequencies, respectively. b1-b3 show the profiles for a model having 12 m uniform fracture spacing. Data are recorded along the x direction. Event 1 is the direct P-wave, events 2 and 3 are respectively the P-to-P reflection from the top and bottom of the fractured layer.

DFM can accurately simulate the geometrical and mechanical properties of individual fractures, while EMM approximates a fractured unit as a locally homogeneously anisotropic rock so that the fracture properties can be inverted from seismic elasticity anisotropy. Accuracy of the EMM based fracture characterization methods may suffer from the effective medium assumption, because natural fractures are unlikely to be uniformly distributed in the earth. To investigate the limitation of EMM in characterizing properties of irregular fracture systems, we use EMM to invert for the fracture spacing from the AVAZ responses obtained from the DFM data. We use EMM to generate a series of AVAZ templates for models of uniform fracture spacing, whose value varies from 0 to 100 m with 0.1 m interval. For the AVAZ obtained from DFM at a given CMP location, we invert for the local fracture spacing by searching through all the templates to find the one that has the minimum root-mean-square error with the data. Fracture compliances are assumed to be known in the inversion.

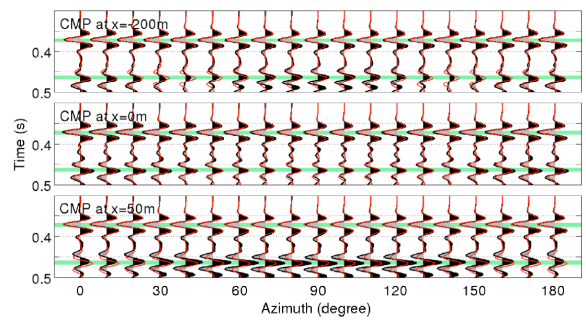

Figure 6. Common offset CMP gathers at x=-200, 0 and 50 m. Black and gray traces are DFM results. Red traces are EMM results. The two green stripes in each plot indicate reflections from the top and bottom of the fractured layer.

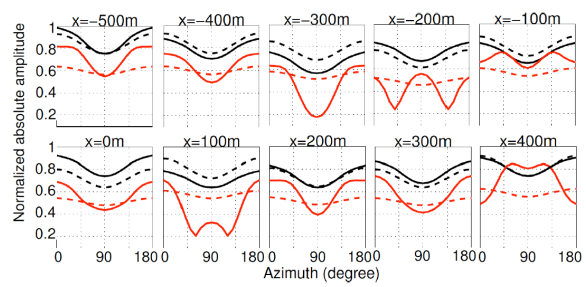

Figure 7. AVAZ responses at 10 different CMP positions. Black and red curves respectively show the AVAZ of reflections from the top and bottom of the fractured layer. Solid and dashed curves are the results obtained from DFM and EMM, respectively.

Figure 8a shows the comparison of the fracture spacing inverted from the AVAZ responses of the reflections from the fractured layer top at 500 m offset and the model mean fracture spacing averaged over the windows of λ (150 m) and 2λ (300m) at each CMP. Figure 8b shows the percentage errors of the inverted spacing with respect to the mean spacing averaged over the two windows together with the standard deviation (STD) of the model fracture spacing at each CMP. The inverted spacing deviates from the true mean spacing by about 10~15% at most CMPs. Variations of the errors shown in Figure 8b are not correlated to the STD (dashed blue curves) of the model fracture spacing. This implies that the difference between inverted spacing

and true mean spacing is not simply determined by the irregularity of the distribution of fractures around each CMP. Figure 9 shows the errors of the spacing inverted from the AVAZ responses of the data recorded at different offsets. At each CMP, the errors of the spacing inverted from the data at different offsets are similar, indicating that the AVAZ responses are consistent at different offsets. We don't show the results for the bottom reflections because we will get incorrect answers if we use the bottom reflections for the inversion as the bottom reflections are strongly influenced by fracture scattering, as shown in Figures 6 and 7.

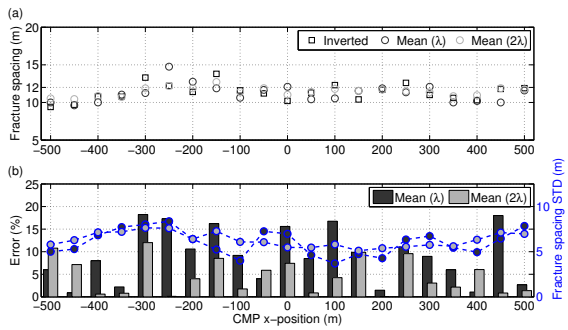

Figure 8. (a) Fracture spacing inverted from AVAZ (squares) and model mean fracture spacing averaged over the ranges of λ (black circles) and 2λ (gray circles) at each CMP position. (b) Black and gray histograms respectively show the percentage error of the inverted fracture spacing with respect to the mean fracture spacing in (a). The two blue dashed lines show the corresponding STD of the fracture spacing within the ranges of λ (black circles) and 2λ (gray circle) at each CMP position, respectively.

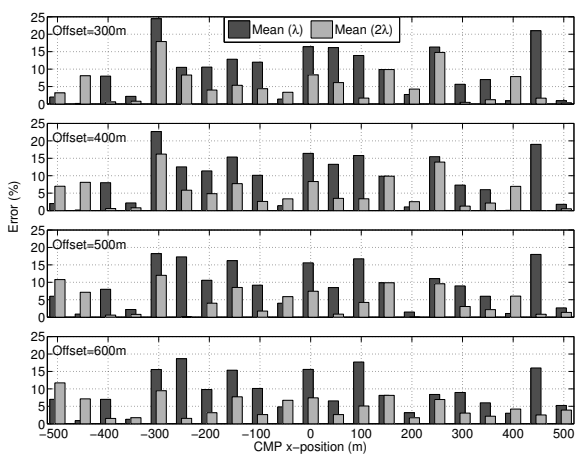

Figure 9. Percentage error of the fracture spacing inverted from the AVAZ responses of the CMP gathers at different offsets. Black and gray histograms show the errors calculated with respect to the mean spacing averaged at each CMP position over the regions of λ and 2λ, respectively.

We simulate 1701 shots with 25 m shot spacing and record the data at the model surface at every 12.5 m. For each common offset azimuthal CMP gather, we stack the data into 18 source bins and 18 receiver bins from 0^0 to 170^0 in steps of 10^0 after normal moveout applied. Figure 10 shows the fracture spacing inverted from the data stacked within bins of different sizes at four different offsets. At short offsets, stacking has very small influence on the fracture spacing inversion. However, at large offsets, the values of the inverted fracture spacing increase with stacking bin size. Overall, stacking has little effect on reducing the errors of the inverted fracture spacing.

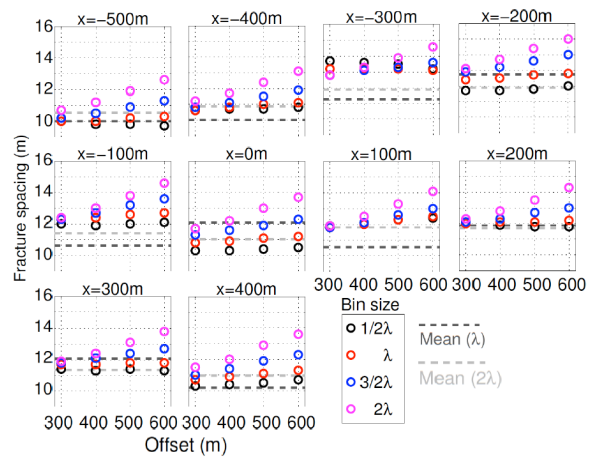

Figure 10. Effect of data stacking on fracture spacing inversion. Black, red, blue and magenta circles respectively represent the fracture spacing inverted from the data stacked within bins of 1/2λ, λ, 3/2 λ and 2 λ width (λ=150 m). Dashed black and gray lines in each panel respectively give the mean fracture spacing averaged over the regions of λ and 2λ centered at the corresponding CMP.

Conclusions

Our modeling results show that clustering of irregularly spaced fractures can significantly affect the characteristics of reflections from a fractured layer and cause the AVOAZ responses to deviate from those predicted by the effective medium theory. Fracture clustering effect can result in more than 10% error in the fracture spacing inversion. Although we only showed the results for one fracture model, we have studied models of different power law distribution (equation 3) and different fracture spacing ranges and reached similar conclusions. Therefore, the accuracy of AVOAZ analysis for fracture characterization may suffer from the effective medium assumption when fractures are irregularly spaced in the earth.

Acknowledgements

We thank Haruo Sato, Stephen Brown and Daniel Burns for discussions about fracture scattering and fractal analysis.

References

Brown, S., and X. Fang, 2012, Fluid flow property estimation from seismic scattering data: 82nd Annual International Meeting, SEG, Expanded Abstracts.

Coates, R.T., and M. Schoenberg, 1995, Finite-difference modeling of faults and fractures: Geophysics, 60(5), 1514-1526.

Daley, T.M., K.T. Nihei, L.R. Myer, E.L. Majer, J.H. Queen, M. Fortuna, J. Murphy, and R.T. Coates, 2002, Numerical modeling of scattering from discrete fracture zones in a San Juan Basin gas reservoir: 72nd Annual International Meeting, SEG, Expanded Abstracts.

Fang, X., M.C. Fehler, Z. Zhu, Y. Zheng, and D.R. Burns, 2014, Reservoir fracture characterization from seismic scattered waves: Geophysical Journal International, 196, 481-492.

Thomsen, L., 1986, Weak elastic anisotropy: Geophysics, 51(10), 1954-1966.

Rüger, A., 1997, P-wave reflection coefficients for transversely isotropic models with vertical and horizontal axis of symmetry: Geophysics, 62(3), 713-722.

Schoenberg, M., 1980, Elastic wave behavior across linear slip interfaces: Journal of the Acoustical Society of America, 68(5), 1516-1521.

Schoenberg, M., and C.M. Sayers, 1995, Seismic anisotropy of fractured rock: Geophysics, 60(1), 204-211.

Willis, M.E., D.R. Burns, R. Rao, B. Minsley, M.N. Toksöz, and L. Vetri, 2006, Spatial orientation and distribution of reservoir fractures from scattered seismic energy: Geophysics, 71(5), O43-O51.

Yang, Z., S. Chi, M.E. Willis, D. Burns, and M.N. Toksöz, 2005, Comparison of discrete fracture and effective media representation of fractures on azimuthal AVO: 75th Annual International Meeting, SEG, Expanded Abstracts.

Zheng, Y., X. Fang, M.C. Fehler, and D.R. Burns, 2013, Seismic characterization of fractured reservoirs by focusing Gaussian beams: Geophysics, 78(4), A23-A28.